Supplementary Information for:

Molecular basis for the acid initiated uncoating of human enterovirus D68

Yue Liu, Ju Sheng, Arno L. W. van Vliet, Geeta Buda,

Frank J. M. van Kuppeveld, and Michael G. Rossmann

Corresponding author: Michael G. Rossmann, e-mail: mr@purdue.edu

This Supplementary Information PDF includes:

Figures S1 – S17

Tables S1 – S11

Supplementary Figures and Figure Legends

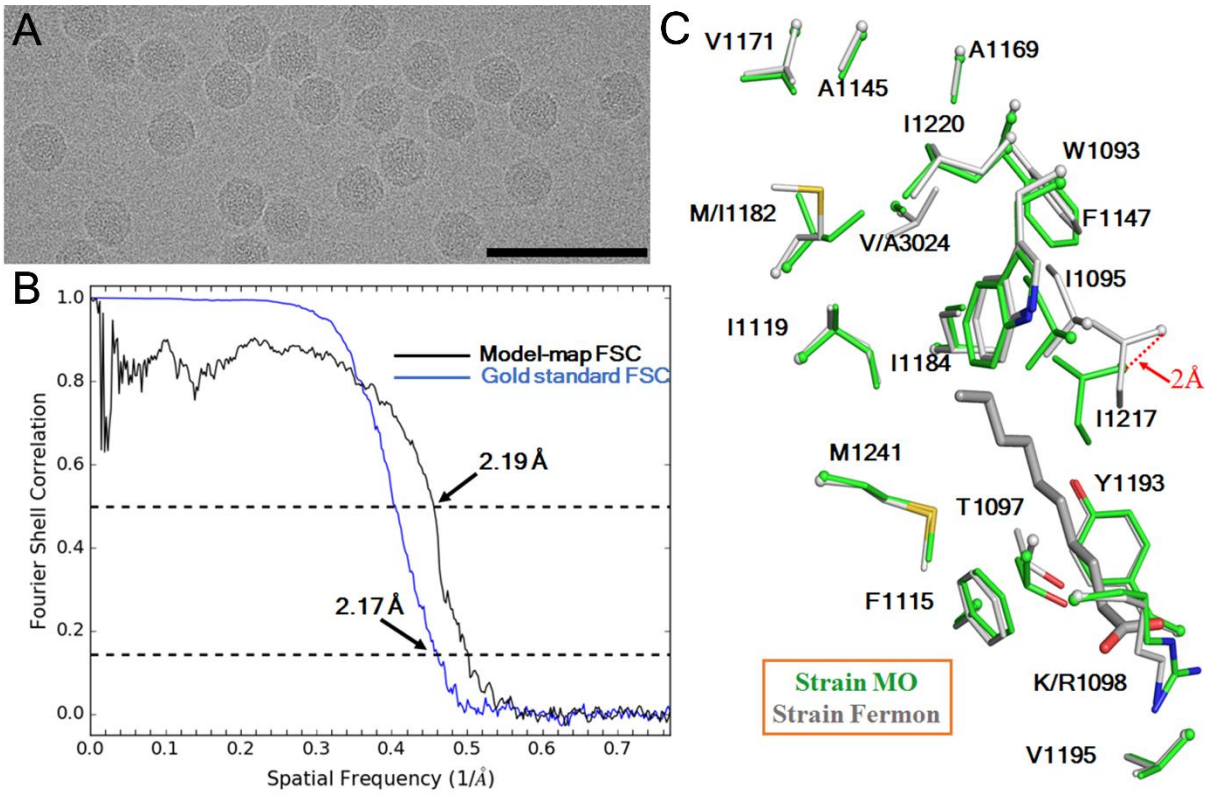

Fig. S1. The cryo-EM structure of EV-D68 strain MO. ***(A)*** A typical portion of an electron micrograph of strain MO. This micrograph was collected at a defocus of 1.3 µm. Scale bar: 100 nm. ***(B)*** Estimation of map resolution based on Fourier shell correlation (FSC) curves. Gold standard FSC refers to the FSC between two independently reconstructed half maps using an FSC cutoff of 0.143 (69,70). Model-map FSC refers to the FSC between the final cryo-EM map and a map calculated based on the atomic model using an FSC cutoff of 0.5 (69). ***(C)*** A close-up view of residues lining the VP1 hydrophobic pockets in strain MO (green) and in strain Fermon (grey). A pocket factor (grey) is present in strain Fermon but is absent in strain MO. In the pocket, these two strains differ mainly in two hydrophobic residues at positions 1182 and 3024. Among 469 EV-D68 strains for which the nearly complete genome sequences are available, the occurrences of Met and Ile at position 1182 are 58% and 42%, respectively. The occurrences of Ala and Val at position 3024 are 52% and 48%, respectively.

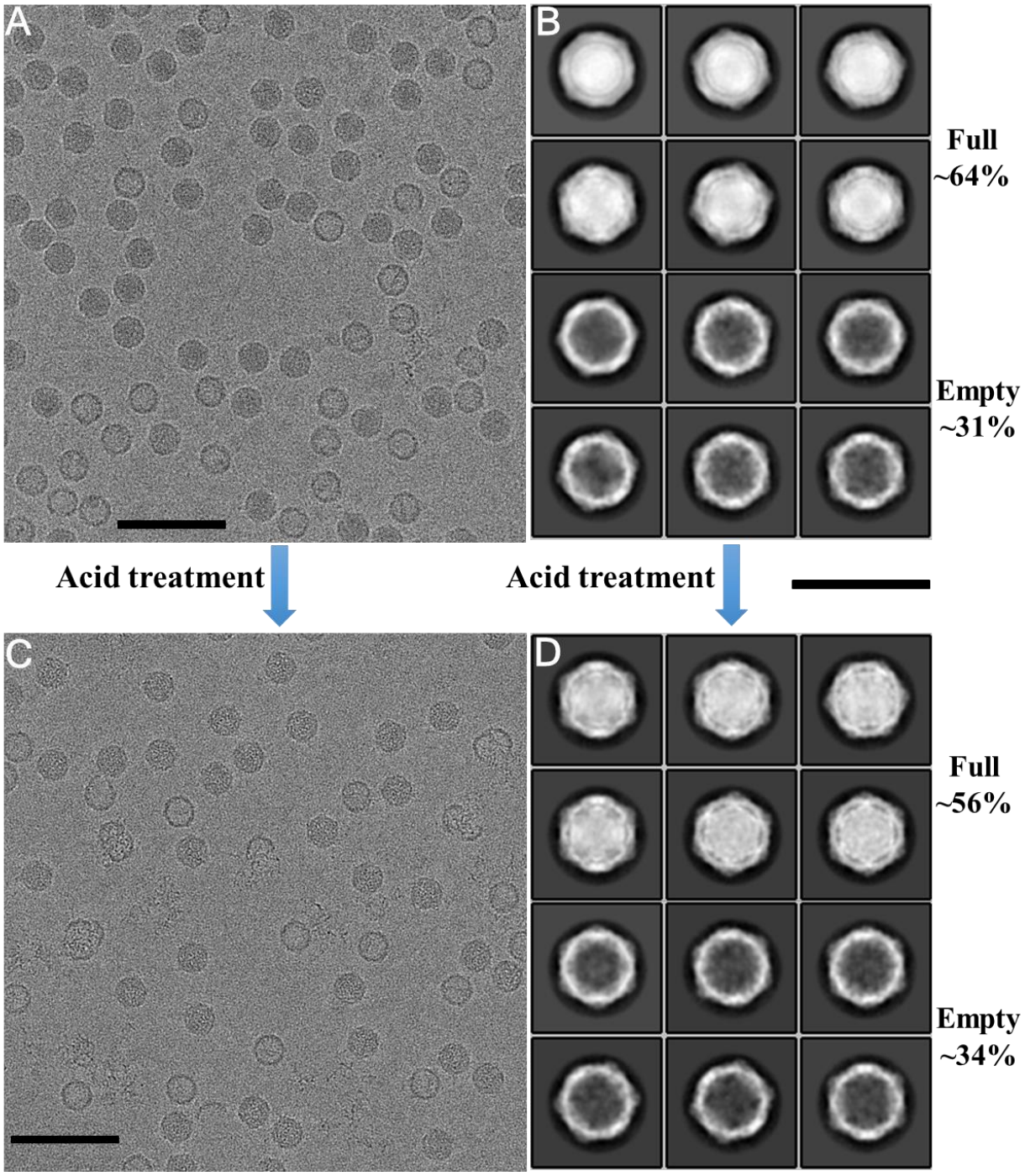

Fig. S2. Acid induces structural alterations of EV-D68 strain MO. Typical electron micrographs show EV-D68 particles that were treated with either a pH 7.2 buffer ***(A)*** or a pH 5.5 buffer ***(C)*** at room temperature for 20 min. Scale bar: 100 nm. The corresponding 2D class averages of particle images are shown in ***(B)*** and ***(D)***, respectively. The percentage of full or empty particles among all particles is given on the right side. The scale bar for ***(B)*** and ***(D)*** represents 50 nm.

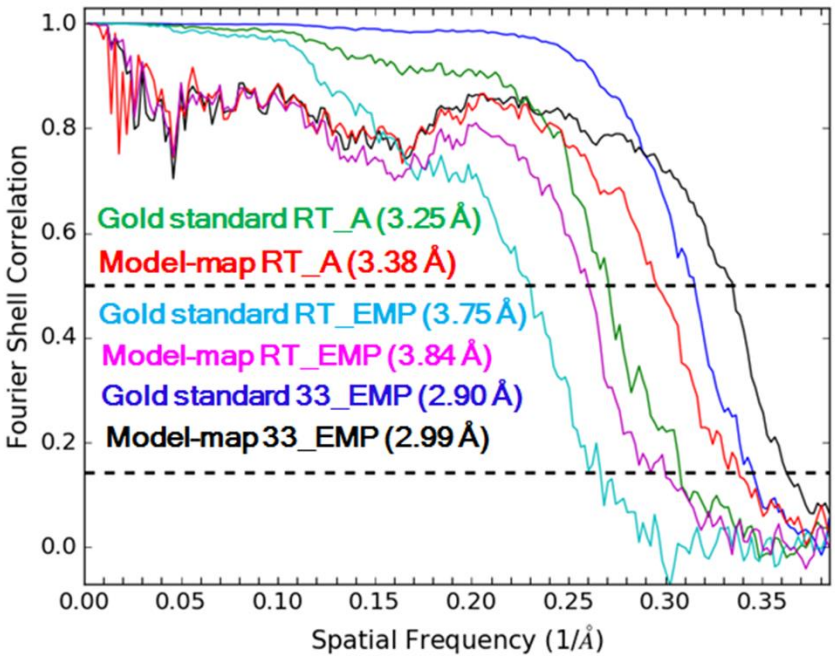

Fig. S3. Assessment of map resolutions based on FSC curves. RT_A and RT_EMP refer to A-particles and emptied particles in dataset B_RT_Acid. 33_EMP refers to emptied particles in dataset B_33_Acid. The FSC curves are defined as in **Fig. S1**.

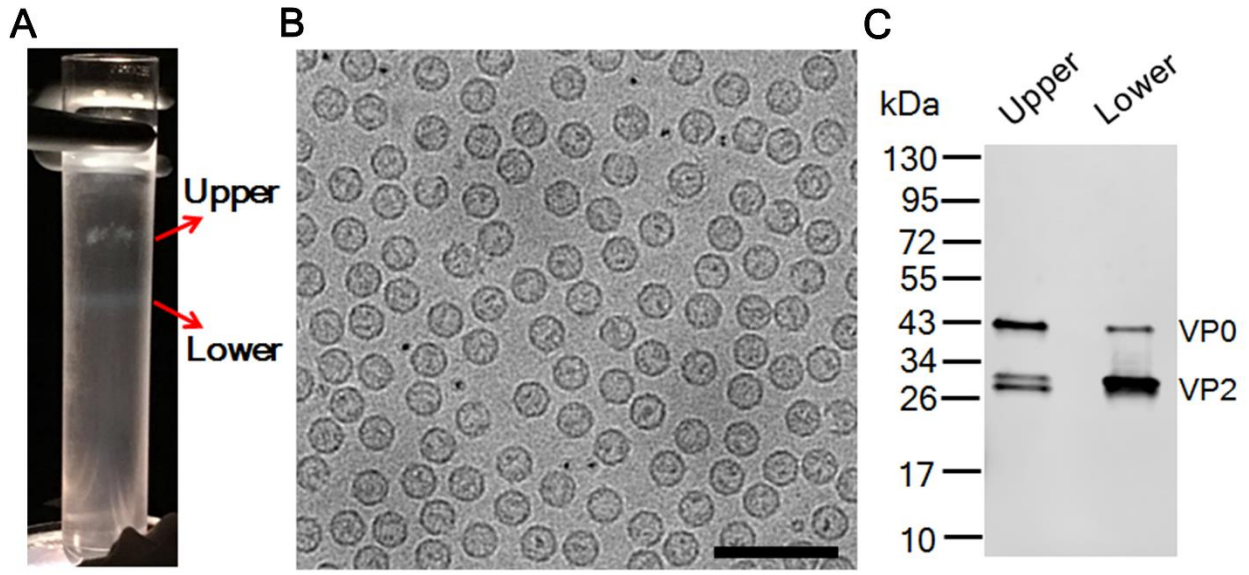

Fig. S4. Purification and characterization of EV-D68 particles. (***A***) Rate zonal ultracentrifugation using a 10%-51% (v/v) iodixanol gradient yields two fractions that contain particles of EV-D68 strain MO. (***B***) A typical cryo-EM micrograph shows that the upper fraction consists of nearly exclusively empty particles. The lower fraction contains a large portion of full particles and is referred to as Prep B as in **Fig. S8**. Scale bar: 100 nm. (***C***) Both fractions were probed for VP0/VP2 content using Western blotting. A rabbit polyclonal anti-EV-D68 VP2 antibody (1:2000, GeneTex) and an IRDye 800CW goat anti-rabbit antibody (1:10000, LI-COR Biosciences) were used as primary and secondary antibodies, respectively. The upper fraction contains procapsids that possess VP0. For the lower fraction, the intensity of the VP2 band is about eight times as strong as that of the VP0 band. Since the ratio between full and empty particles in Prep B is about 1.9:1, VP0-contaning procapsids account for only a small portion of empty particles in PrepB, whereas VP2-containing emptied particles represent a large portion of empty particles. This is in agreement with 3D classification results shown in **Fig. S8**.

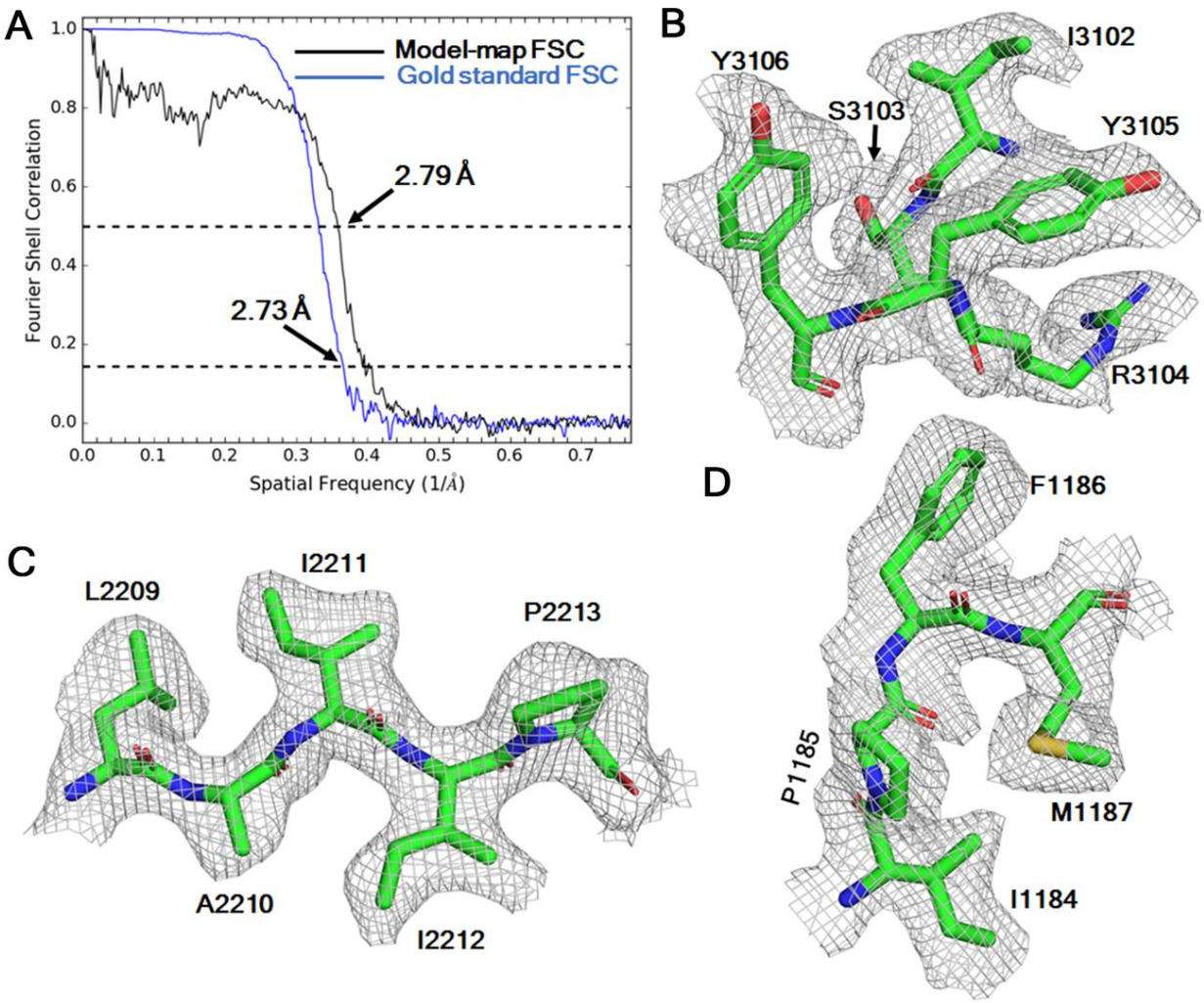

Fig. S5. The 2.7 Å resolution structure of A-particles. ***(A)*** The resolution of the cryo-EM map was estimated based on FSC curves, defined as in **Fig. S1**. ***(B-D)*** Typical densities of the cryo-EM map with the fitted atomic model.

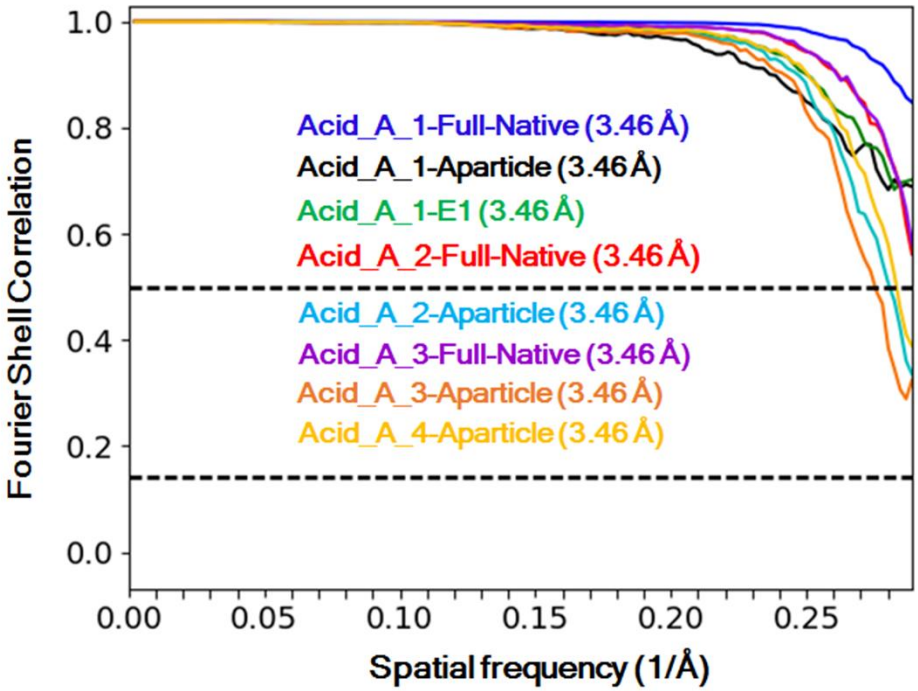

Fig. S6. Assessment of map resolutions for datasets Acid_A_1, Acid_A_2, Acid_A_3, and Acid_A_4 based on FSC curves. The FSC curves are defined as in **Fig. S1**.

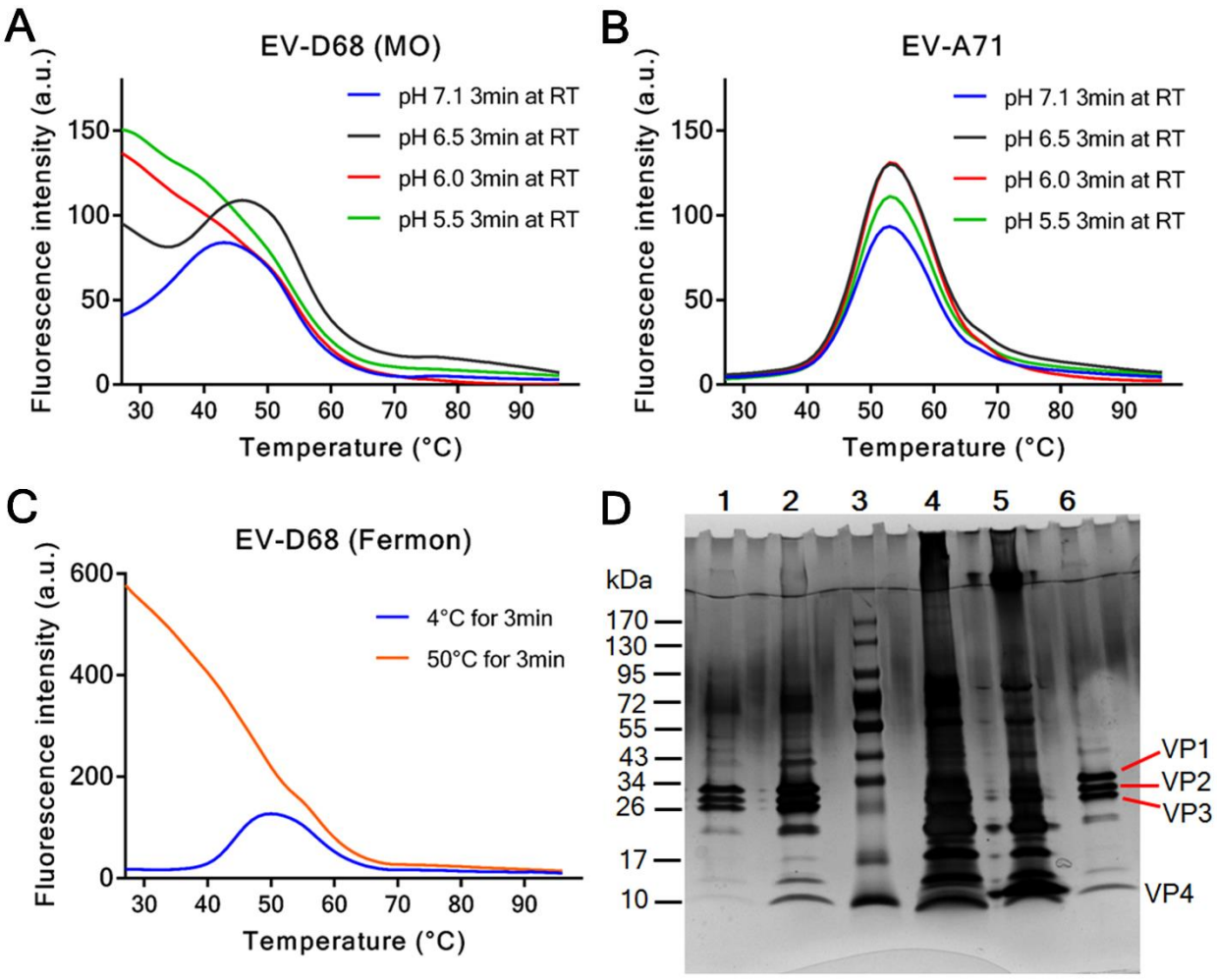

Fig S7. Acid induced structural changes facilitate EV-D68 uncoating. (***A***-***C***) The exposure of genomic RNA upon increase of temperature was monitored by RNA-binding Sybr Green II dye. The mean fluorescence intensity of triplicate measurements is plotted as a function of temperature. Samples were treated under indicated conditions before being quenched and used for thermostability assays. (***A***) Upon acid treatments, the genomic RNA of EV-D68 strain MO becomes more exposed at low temperatures. The curve for pH 6.5 shows a two-stage transition of RNA exposure, which is not apparent under lower pH conditions. This is in agreement with a partial conversion of full native virions to A-particles at pH 6.5 shown by cryo-EM analyses. At low temperatures, the porous structure of A-particles confers accessibility of genomic RNA to dye molecules. The genome becomes fully exposed at a high temperature due in large part to heat triggered uncoating of full native virions. (***B***) The thermal stability of acid resistant EV-A71 remains nearly unchanged when varying pH condition. (***C***) Heating of EV-D68 strain Fermon

results in A-particles and probably also RNA release from a portion of virions. The temperature at which genomic RNA is exposed, Tr (**Materials and Methods**), for strains MO and Fermon is about 37°C and 45°C, respectively. (***D***) SDS-PAGE analysis employing a 4–20% Mini-PROTEAN TGX gel (silver stained, Bio-Rad). Lane 1: acid treated EV-D68 strain MO. Prep A was treated with a pH 5.5 buffer for 20 min at RT and neutralized back using a sufficiently excessive amount of buffer 1 (100mM Na_2HPO_4 and 50mM citric acid, pH 7.6). The resultant sample was subjected to buffer exchange into buffer 1 using an Amicon Ultra centrifugal filter (100 kDa molecular weight cutoff). This enabled removal of VP4 molecules that are not associated with viral particles. Lane 2: control Prep A (without acid treatment) that was concentrated using the same type of centrifugal filter. Lane 3: marker; lane 4: empty particles derived from the upper fraction. Lanes 5 and 6 represent a diluted version of samples in lanes 4 and 2, respectively. The calculated molecular weights of VP1, VP2, VP3, and VP4 are 32.9 kDa, 27.5 kDa, 27.1 kDa, and 7.5 kDa. Acid treatment of Prep A leads to loss of a majority of VP4 from viral particles, as is evident from comparison of lanes 1 and 6.

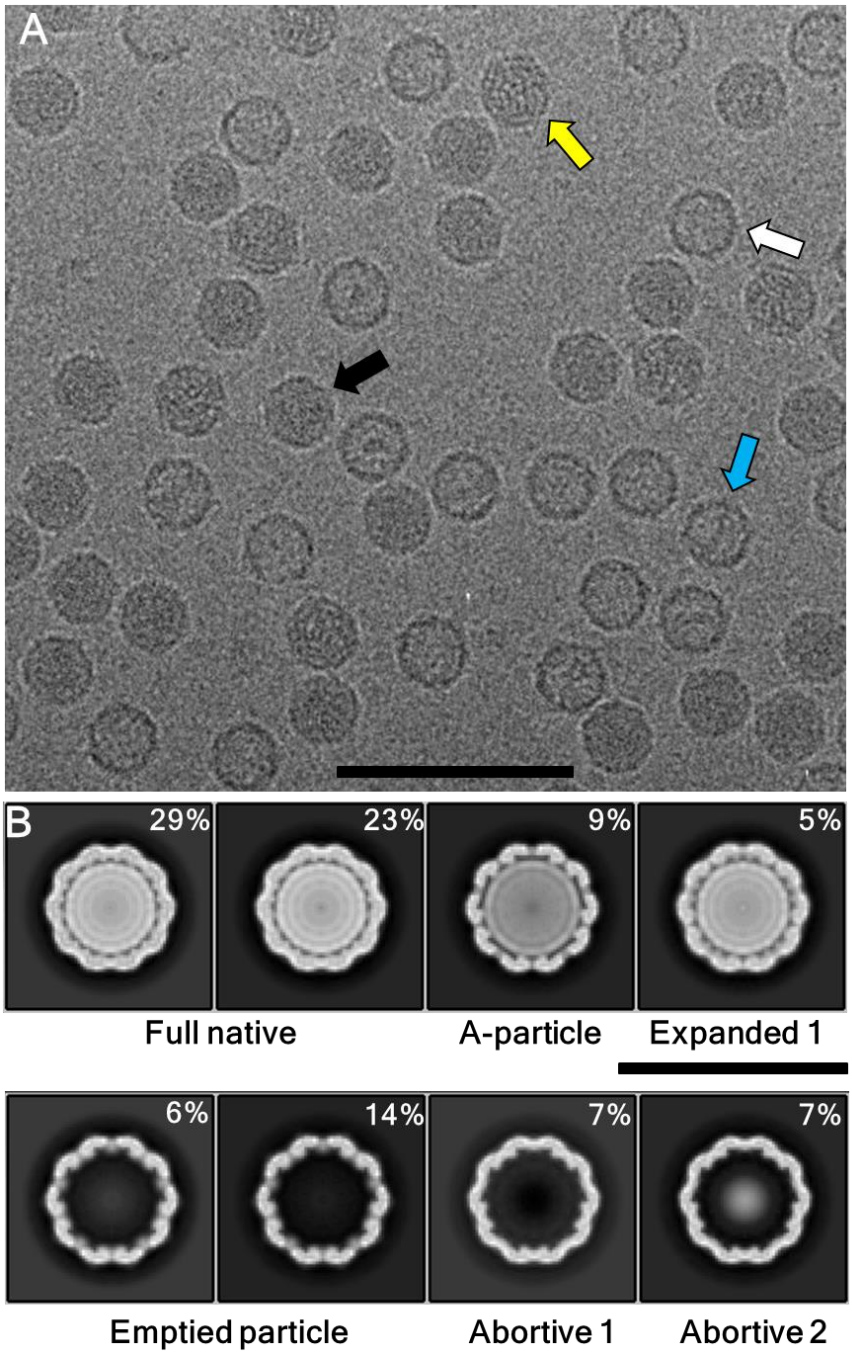

Fig S8. Cryo-EM analyses of a mixed population of EV-D68 particles demonstrate the presence of multiple distinct structural states. ***(A)*** A typical electron micrograph of EV-D68 particles kept at 4°C and at pH 7.2. Arrows with different colors indicate distinct particle forms judged by visual inspection. Scale bar: 100 nm. ***(B)*** Three-dimensional (3D) reconstructions obtained after 3D classification show differences between structural states. The central slice of each

reconstruction is shown. The percentage of particles, which were used for each reconstruction, among all particles is given at the upper right corner. Scar bar: 50 nm.

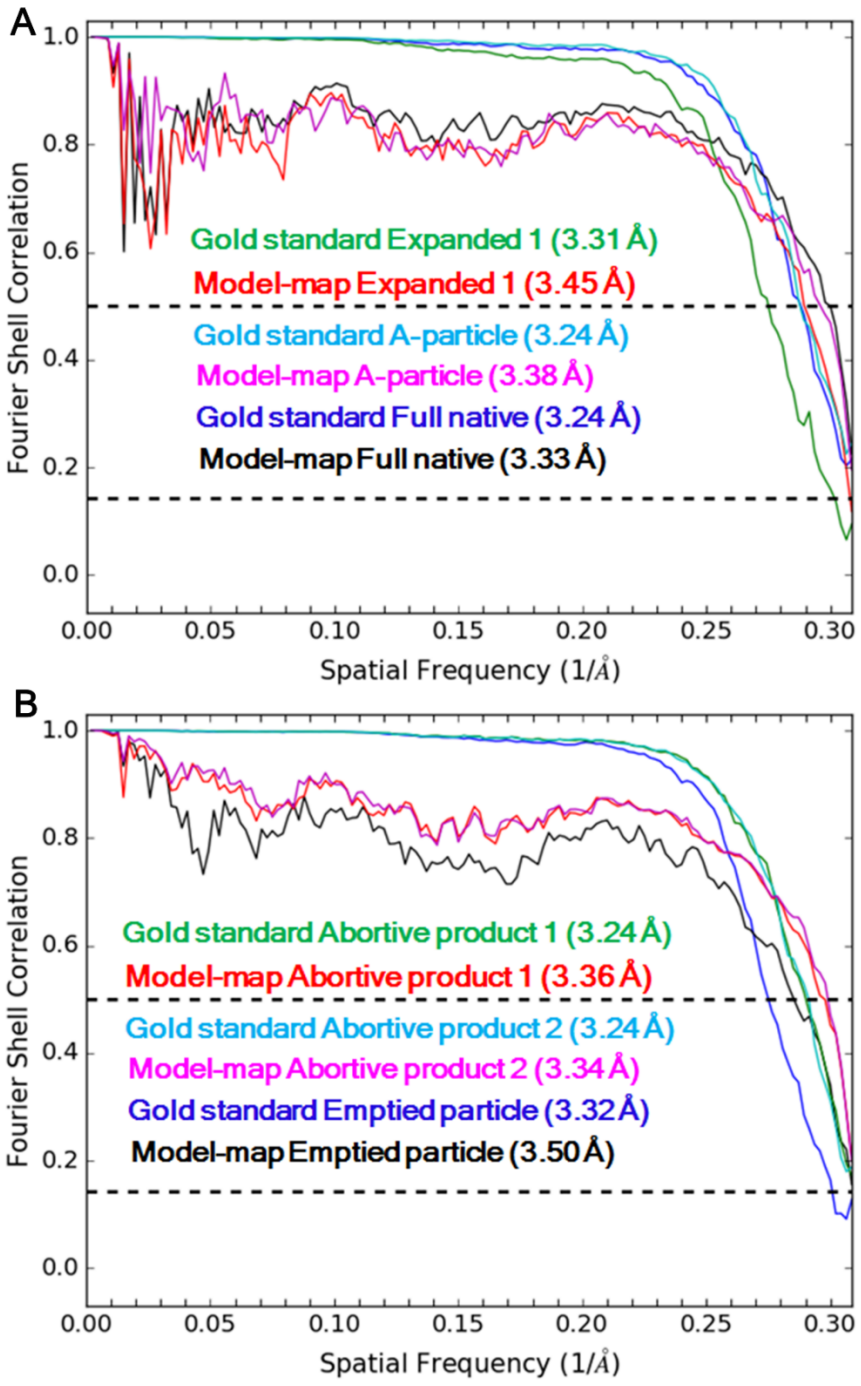

Fig. S9. Assessment of the resolution of cryo-EM maps (dataset B_4_Neu) based on FSC curves. Shown are FSC curves for each of the three full particle states ***(A)*** and those for each of the three empty particle states ***(B)***. Gold standard FSC and model-map FSC are defined as in **Fig. S1**.

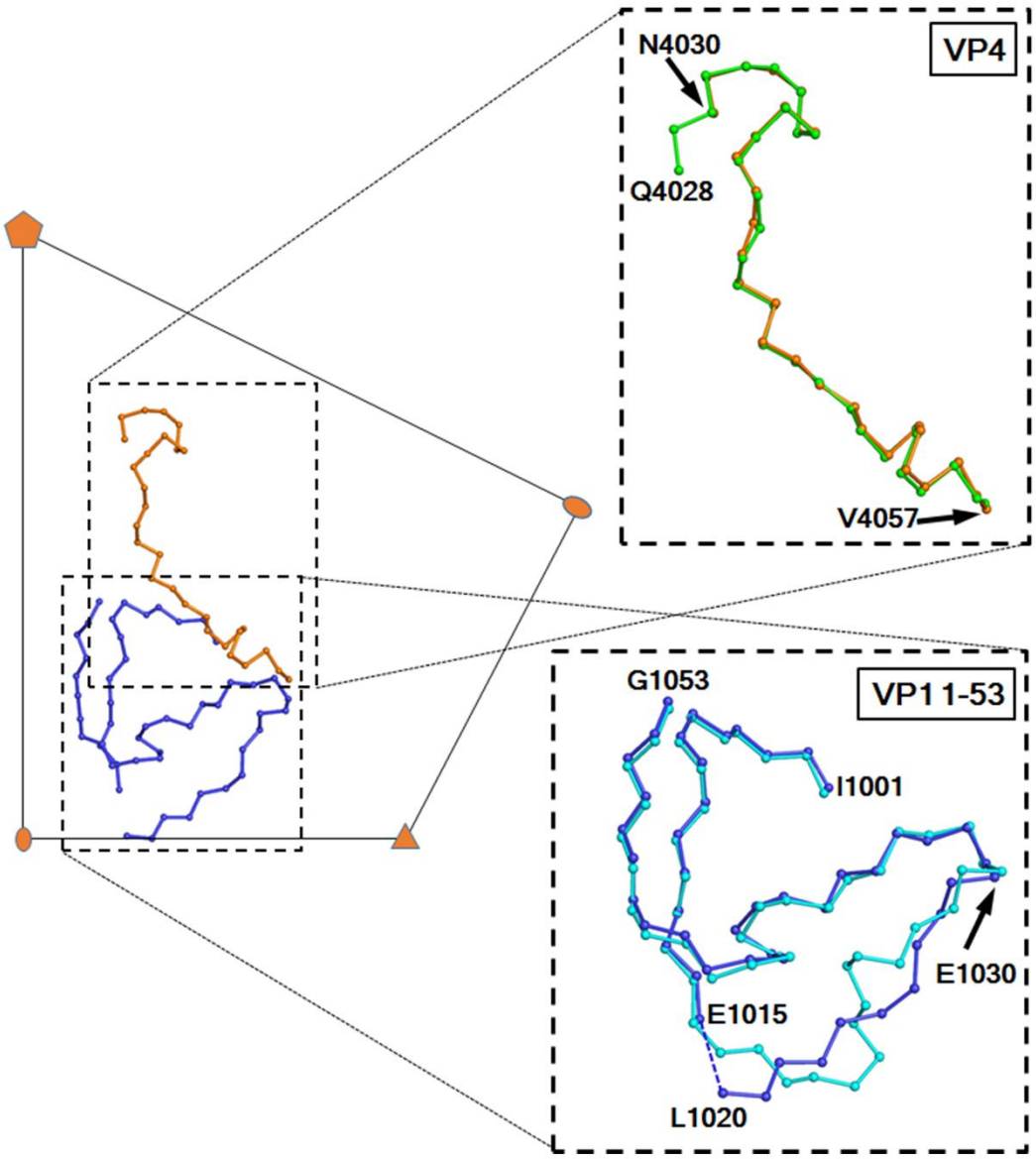

Fig. S10. Structural comparison of the ordered VP1 N-terminal residues and VP4 when superimposing equivalent protomers in full native virions and E1 particles. The left part of this figure shows a protomer of the E1 particle structure. Two rectangles (dashed line) indicate the limit of close-up views on the right. Upper right rectangle: Cα backbone trace of the ordered VP4 residues in full native virions (4028-4057, green) and E1 particles (4030-4057, orange). Lower right rectangle: Cα backbone trace of the ordered VP1 N-terminal residues in full native virions (cyan) and E1 particles (blue). Residues 1016-1019 are disordered in E1 particles. The two structures differ mainly in residues 1020-1029. This leads to destabilization of the virus as illustrated in **Fig. S13**.

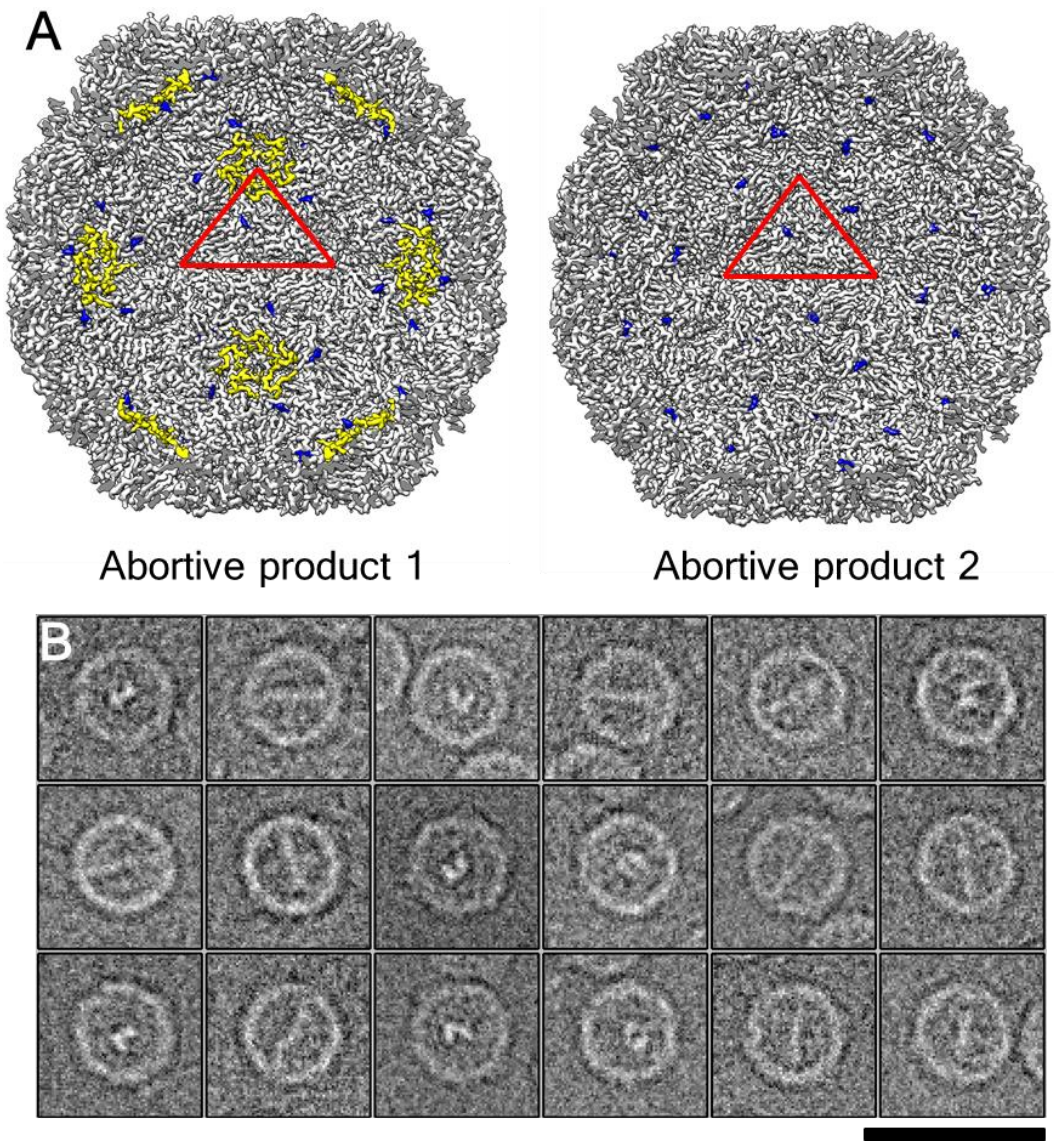

Fig. S11. Multiple structural states of EV-D68 are present at neutral pH. ***(A)*** Cut-way views of two structural states, which probably represent abortive products during EV-D68 assembly, when looking into the particle along an icosahedral two-fold axis. A red triangle indicates an icosahedral asymmetric unit. The internal regions are colored as in **Fig. 3**. ***(B)*** Typical cryo-EM images of abortive product 2 particles that show rod-like inner densities. Scale bar: 50 nm.

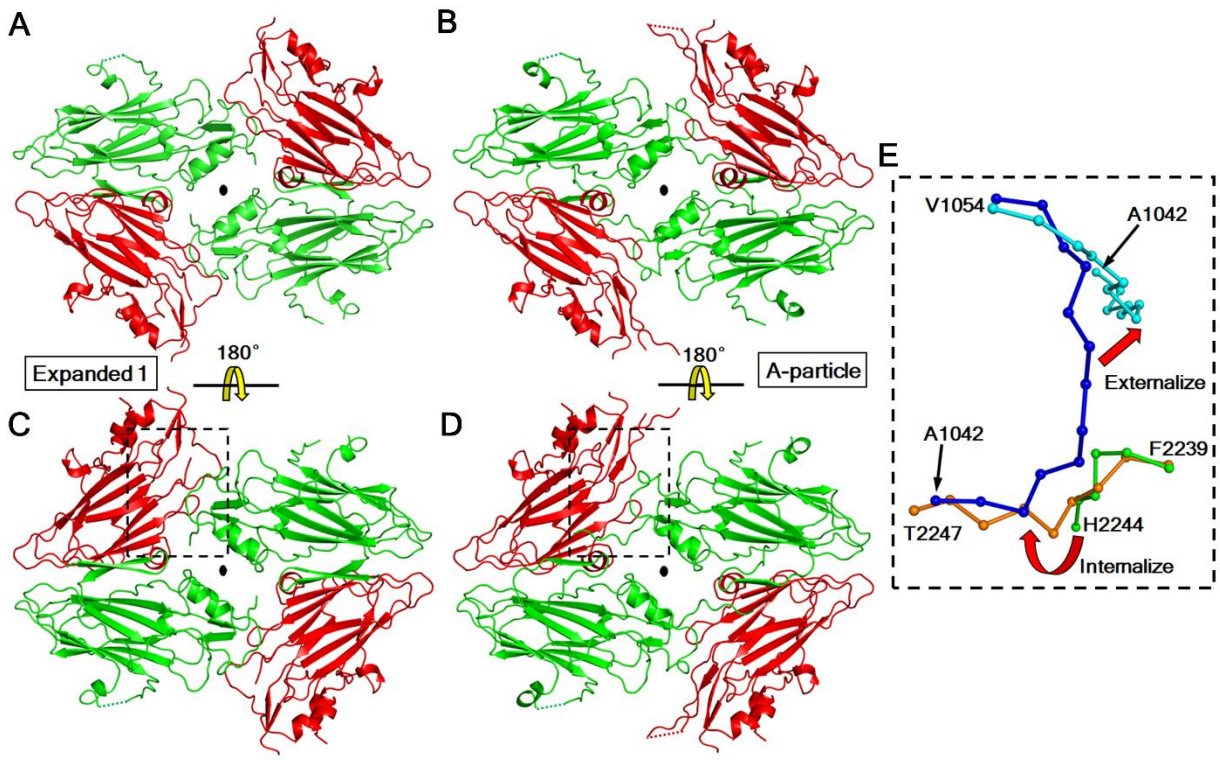

Fig. S12. Structural rearrangements around the icosahedral two fold axes when E1 particles are converted into A-particles. ***(A-D)*** Pores are open around the two-fold axes in the E1 particles (***A***, ***C***) and A-particles (***B***, ***D***). Shown are VP2 (green) and VP3 (red) when viewing the particle through an icosahedral two-fold axis. Either the outer surface (***A-B***) or the inner surface (**C-D**) of the particle points towards the viewer. ***(E)*** A major difference around the two fold axes between these two types of particles lies in the VP2 C-terminus when superimposing equivalent protomers of the E1 particles (VP1: blue, VP2: green) and A-particles (VP1: cyan; VP2: orange). The limit of this close-up view corresponds to that outlined by a rectangle in ***C*** and in ***D***. When the E1 particles are converted into the A-particles, internalization of the VP2 C-terminal tails promotes the externalization of the VP1 N-termini.

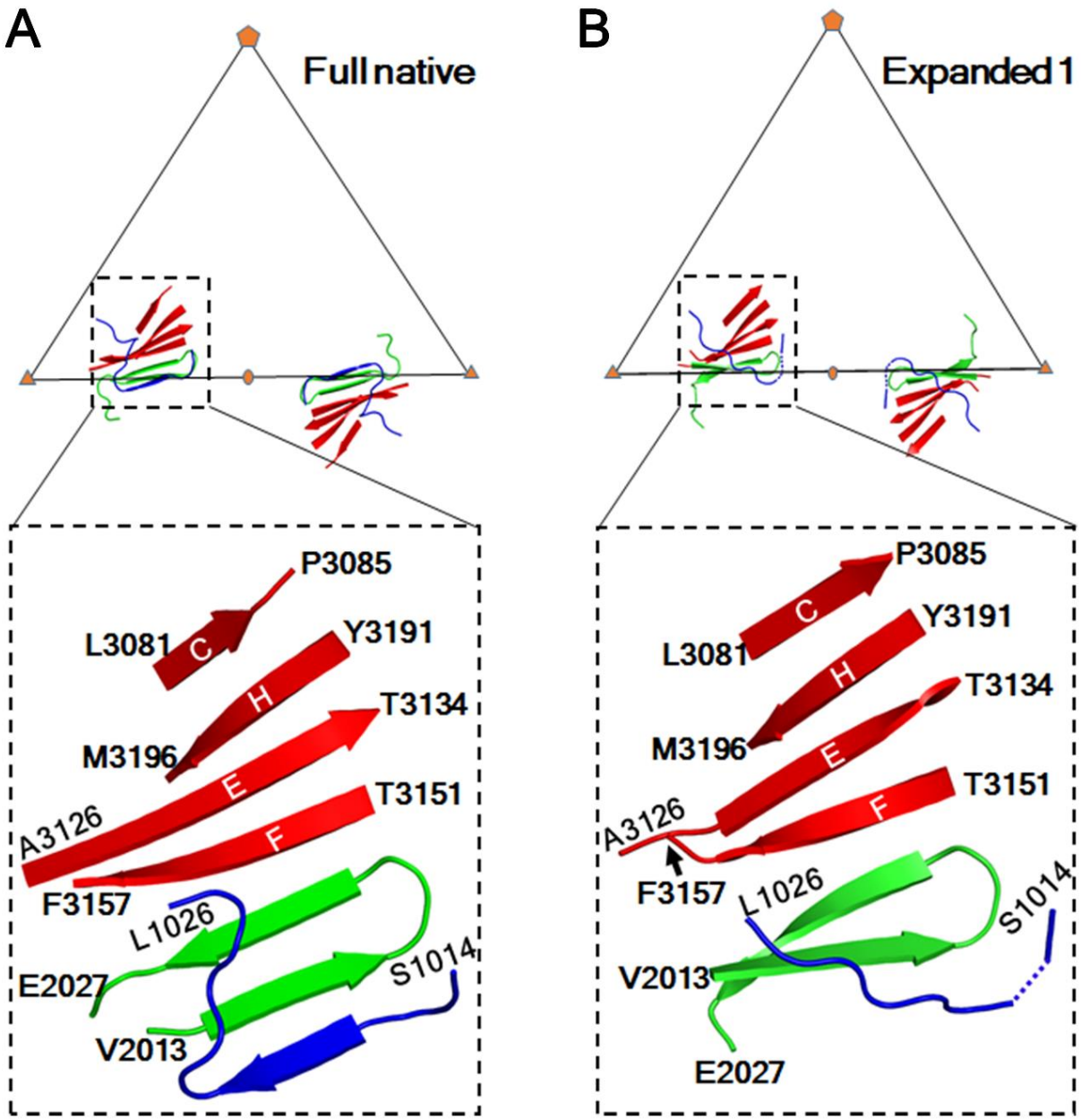

Fig. S13. The seven-stranded interpentamer sheets in full native virions ***(A)*** are partially disrupted in E1 particles ***(B)***. Each triangle indicates an icosahedral asymmetric unit. VP1, VP2, and VP3 are colored blue, green, and red, respectively. In each panel, a rectangle (dashed line) in the upper triangle defines the limit of the close-up view in the large bottom rectangle (dashed line), which is slightly tilted for better visualization. The β-strands C, H, E, and F in VP3 are labelled by their corresponding letters. Residues 1016-1019 are disordered in the E1 particle structure.

Full native			Expanded 1			A-particle		
Chain	Residue No.	Residue	Chain	Residue No.	Residue	Chain	Residue No.	Residue
A7	1014	SER	A7	1021	GLY	B6	2242	LEU
A7	1015	GLU	A7	1022	VAL	B6	2244	HIS
A7	1016	ILE	A7	1023	VAL	B6	2245	ALA
A7	1017	ASN	A7	1024	PRO	B6	2247	THR
A7	1018	ALA	A7	1026	LEU	C7	3150	GLY
A7	1019	GLU	A7	1042	ALA	C7	3151	THR
A7	1020	LEU	C7	3150	GLY	C7	3152	HIS
A7	1021	GLY	C7	3151	THR	C7	3153	ILE
A7	1023	VAL	C7	3152	HIS	C7	3154	VAL
A7	1024	PRO	C7	3153	ILE	C7	3155	TRP
A7	1025	SER	C7	3154	VAL	C7	3159	LEU
A7	1026	LEU	C7	3155	TRP	C7	3160	GLN
A7	1040	GLU	C7	3159	LEU	C7	3163	VAL
A7	1041	GLU	C7	3160	GLN			
A7	1042	ALA						
A7	1043	ILE						
A7	1044	GLN						
B6	2242	LEU						
C7	3128	LYS						
C7	3149	LEU						
C7	3150	GLY						
C7	3151	THR						
C7	3152	HIS						
C7	3153	ILE						
C7	3154	VAL						
C7	3155	TRP						
C7	3156	ASP						
C7	3158	GLY						
C7	3159	LEU						
C7	3160	GLN						
C7	3163	VAL						

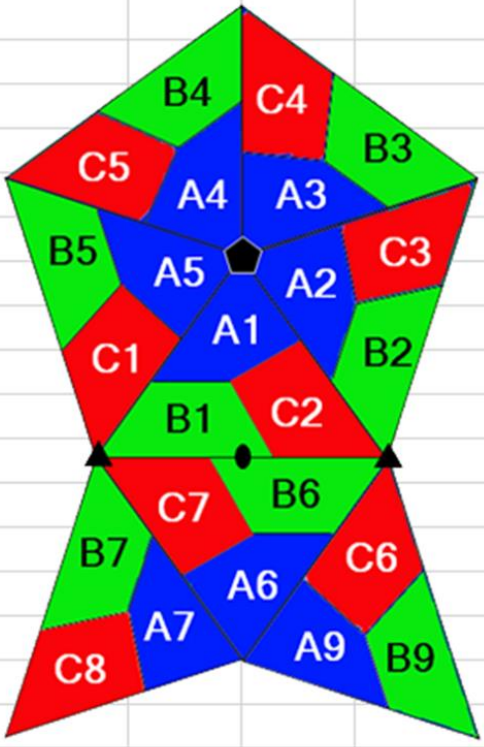

Fig. S14. Structural reorganization of the VP2 N-termini weakens the interpentamer contact during uncoating. A schematic (bottom right) of eight icosahedral asymmetric units of the capsid is colored blue (VP1), green (VP2), and red (VP3). Each subunit is labelled by a chain number

(e.g., A1). For each of the three full particle states (dataset B_4_Neu), the residues listed above are within a distance of 4 Å to any atom of residues 2013-2026 in chain B1.

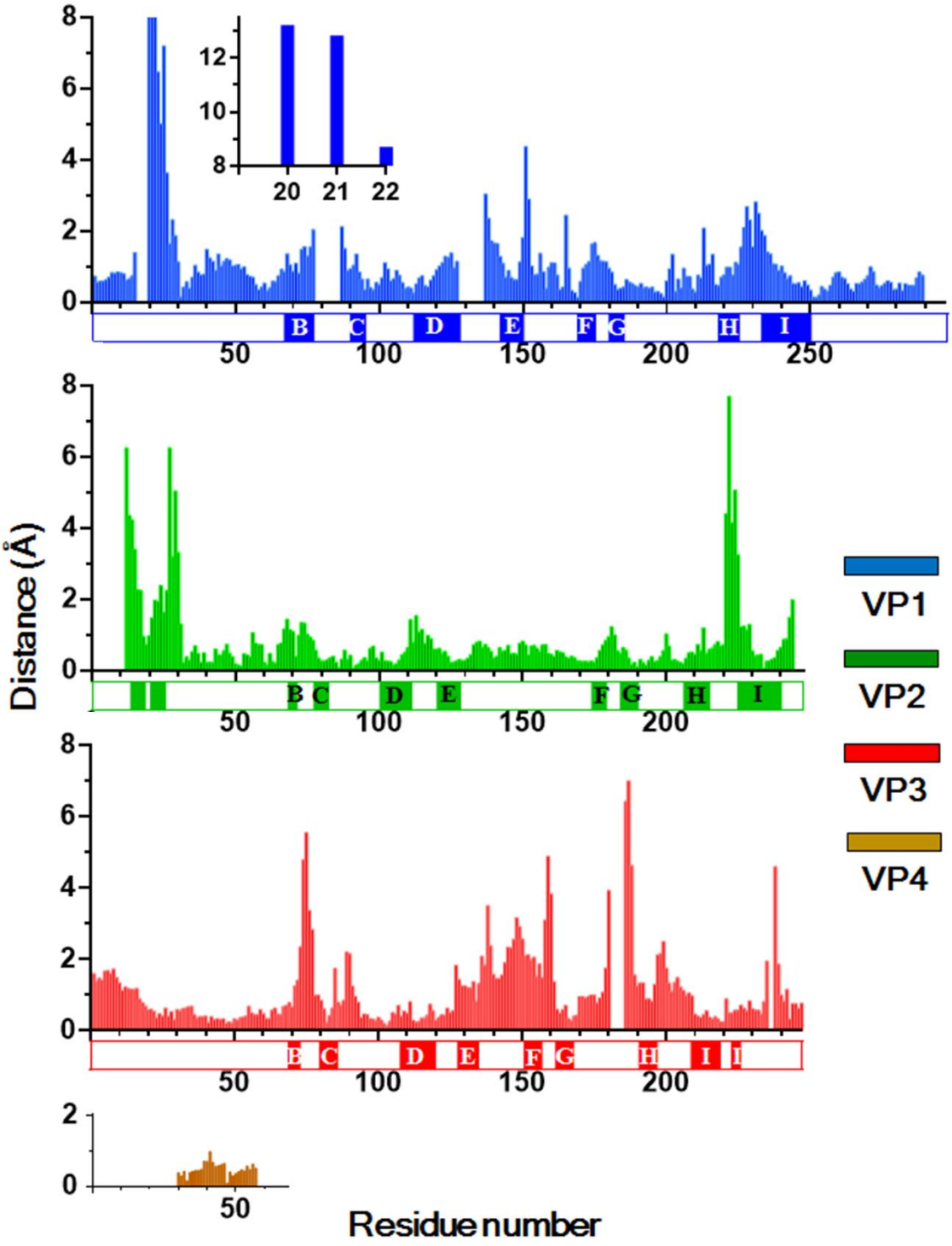

Fig. S15. Distances between equivalent Cα atoms upon superposition of equivalent protomers in full native virions and E1 particles. Rectangular blocks denote residues that form β-strands. The

jelly roll β-strands B, C, D, E, F, G, H, and I are labelled by their corresponding letters. The inset shows a close-up view of the plot for the VP1 N-terminal residues 1020-1022.

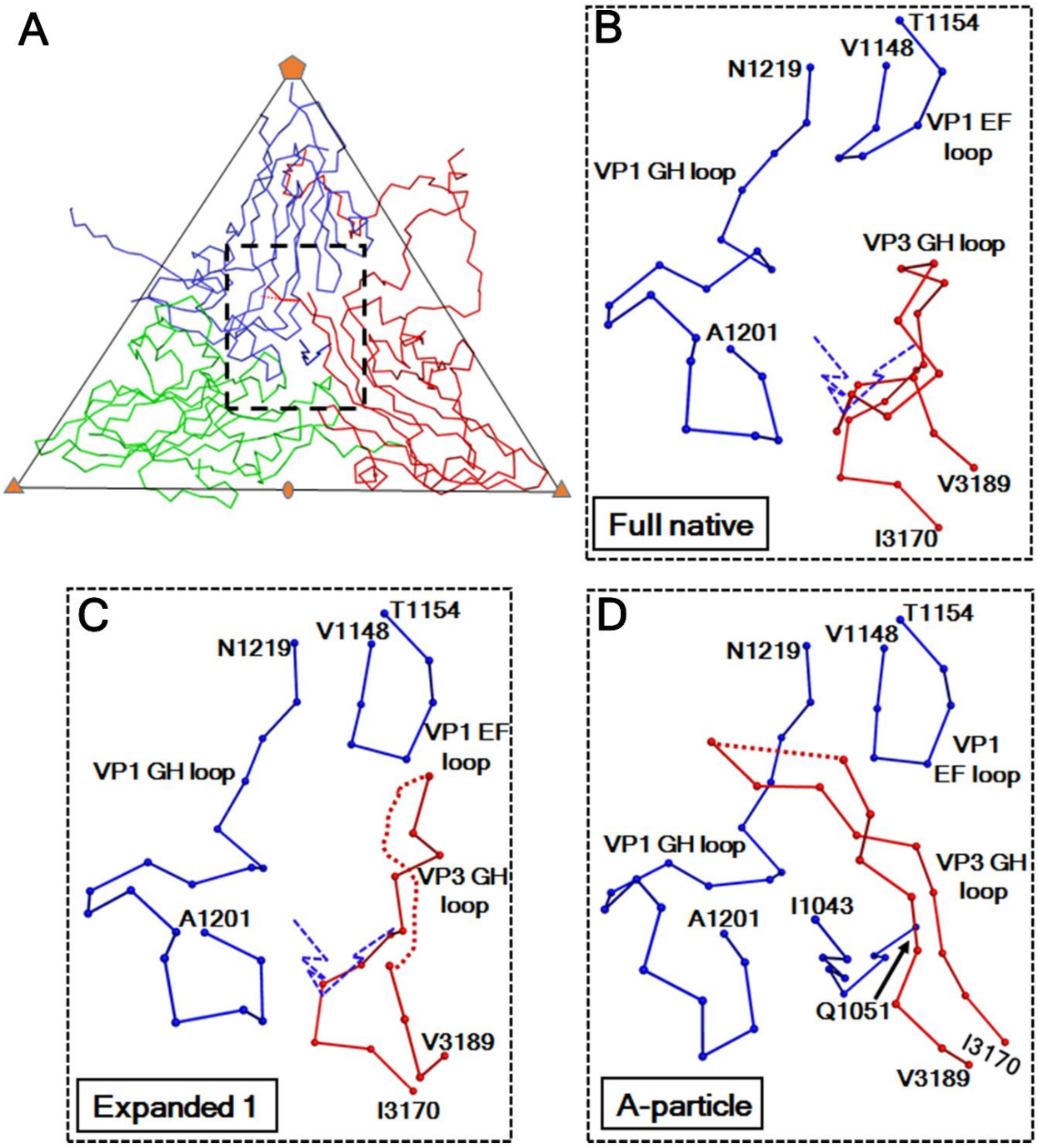

Fig. S16. Structural rearrangements of loops near the quasi-three-fold axes facilitate the externalization of the VP1 N-termini. ***(A)*** The Cα backbone representation of an icosahedral asymmetric unit of the A-particle structure is colored blue (VP1), green (VP2), and red (VP3). The rectangle (dashed line) indicates the limit of the close-up views in ***(B-D)***. ***(B)*** The structure of full native virions after superimposition of equivalent protomers in full native virions and A-

particles. ***(C)*** The structure of E1 particles after superimposition of equivalent protomers in E1-particles and A-particles. In these two panels, a blue dashed line represents the Cα backbone trace of the VP1 N-terminal residues 1043-1051 observed in the A-particle structure. These residues would clash with the VP3 GH loop in full native virions and with that in E1 particles. The VP3 GH loop adopts a coiled conformation in full native virions. This loop becomes partially disordered and adopts a more extended conformation in the other two structural states.

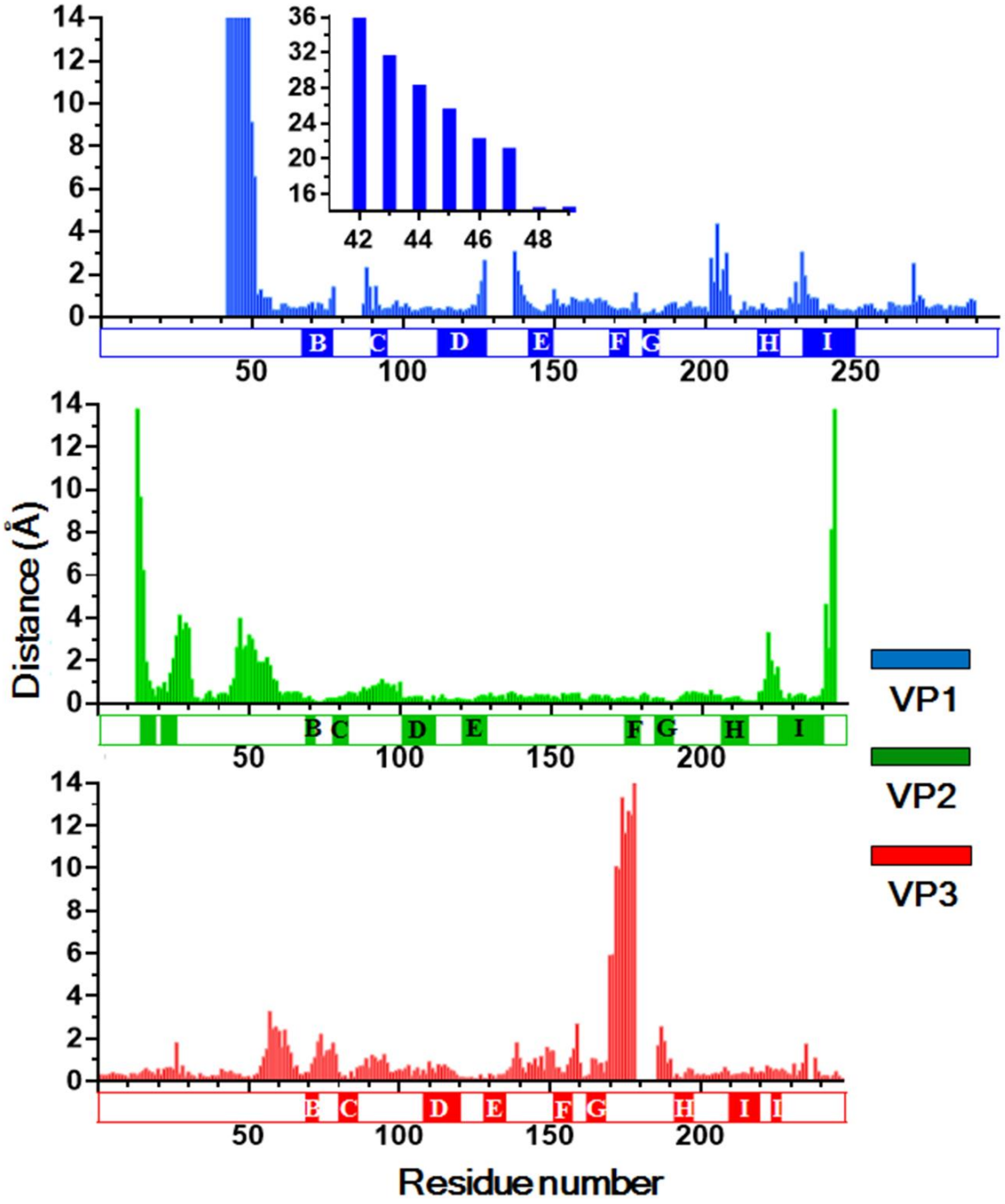

174

175 **Fig. S17.** Distances between equivalent Cα atoms upon superposition of the equivalent
176 protomers in E1 particles and A-particles. The rectangular blocks are defined as in **Fig. S13**. The
177 inset shows a close-up view of the plot for the VP1 N-terminal residues 1042-1049.

178

Table S1. Cryo-EM data statistics.

	A_Native (full)	B_RT_Acid (A-particle)	B_RT_Acid (emptied)	B_33_Acid (A-particle)	B_33_Acid (emptied)
Data collection and processing[a]					
No. of micrographs[b]	642	144	144	950	950
Pixel size[c] (Å/pixel)	0.65	0.65	0.65	0.65	0.65
Dose rate (e-/pixel/s)	8	8	8	8	8
Total dose (e-/Å^2)	36	28	28	38	38
Frame rate (ms)	200	200	200	200	200
Defocus (μm)	0.3-3.0	0.9-4.8	0.9-4.8	0.5-3.5	0.5-3.5
No. of ptcls for reconstruction	16021	3708	2150	23082	19325
Resolution[d] (Å)	2.17	3.25	3.75	2.73	2.90
Map sharpening B-factor (Å^2)	-83.0	-125.7	-163.7	-120.2	-144.1
Model Statistics					
Correlation coefficient[e]	0.838	0.834	0.829	0.848	0.846
No. of atoms					
Protein	6822	5362	5025	5579	5083
Water	493	0	0	252	0
Avg. B-factor (Å^2)	18.2	39.9	49.2	30.4	32.5
r.m.s deviations[f]					
Bond lengths (Å)	0.010	0.009	0.008	0.010	0.011
Bond angles (°)	1.355	1.261	1.151	1.327	1.261
Ramachadran plot[f]					
Favored (%)	96.1	94.0	91.7	94.7	93.6
Allowed (%)	3.6	5.8	7.8	5.0	5.9
Outliers (%)	0.3	0.2	0.5	0.3	0.5

[a] Cryo-EM data were collected using an FEI Titan Krios transmission electron microscope operated at 300 kV and equipped with a Gatan K2 Summit direct electron detector.
[b] Micrographs from which particles were selected.
[c] Super resolution pixel size. The physical pixel size is 1.3 Å/pixel.
[d] Estimated based on Fourier shell correlation between two half maps using a cutoff of 0.143 (69).
[e] Between the cryo-EM map and a map calculated based on the atomic model specifying the cryo-EM map resolution.
[f] Based on the criteria of MolProbity (76).

Table S2. Root-mean-square deviations (Å) between pairs of EV-D68 structures.[a]

	Native_full[b]	RT_A[c]	RT_EMP[c]	33_A[d]	33_EMP[d]
Native_full[b]	-				
RT_A[c]	5.7	-			
RT_EMP[c]	4.6	0.8	-		
33_A[d]	5.7	0.6	0.7	-	
33_EMP[d]	4.6	0.7	0.6	0.5	-

[a] Calculated based on equivalent Cα atoms when icosahedral symmetry axes are aligned.
[b] Dataset A_Native.
[c] Dataset B_RT_Acid. A and EMP refer to A-particle and emptied particle, respectively.
[d] Dataset B_33_Acid. A and EMP refer to A-particle and emptied particle, respectively.

Table S3. Root-mean-square deviations[a] between pairs of structures that belong to the same structural state.

Structure A	Structure B	r.m.s.d (Å)	# of equivalent Cα atoms
A_Native-full	B_4_Neu-Full-Native	0.5	800
B_RT_Acid-Aparticle	B_33_Acid-Aparticle	0.6	679
B_4_Neu-Aparticle	B_RT_Acid-Aparticle	0.7	685
B_4_Neu-Aparticle	B_33_Acid-Aparticle	0.8	679
B_RT_Acid-Emptied	B_33_Acid-Emptied	0.6	638
B_4_Neu-Emptied	B_RT_Acid-Emptied	0.7	639
B_4_Neu-Emptied	B_33_Acid-Emptied	0.6	643
B_4_Neu-E1	A_Acid_1-E1	0.5	768

[a] Calculated based on equivalent Cα atoms upon superposition of equivalent protomers in each pair of structures.

Table S4. CryoEM data statistics.

	A_1[a]	A_1[a]	A_1[a]	A_2[a]	A_2[a]	A_3[a]	A_3[a]	A_4[a]
Temperature	4	4	4	RT	RT	RT	RT	RT
pH	6.5	6.5	6.5	6.5	6.5	6	6	6
Time[b]	3min	3min	3min	3min	3min	30s	30s	3min
Structural state[c]	Native	E1	A-	Native	A-	Native	A-	A-
No. of micrographs[d]	357	357	357	774	774	884	884	118
Defocus[e] (μm)	0.5-8.5	0.5-8.5	0.5-8.5	0.5-7.0	0.5-7.0	1.1-5.4	1.1-5.4	1.7-5.7
Pixel size (Å/pixel)	1.73	1.73	1.73	1.73	1.73	1.73	1.73	1.73
Dose rate (e^-/pixel/s)	8	8	8	8	8	8	8	8
Frame rate (ms)	250	250	250	250	250	250	250	250
Total dose (e^-/ Å^2)	28	28	28	28	28	28	28	28
# particles for reconstruction	15000	4968	2324	16000	14000	16000	14000	19798
Resolution[f] (Å)	3.46	3.46	3.46	3.46	3.46	3.46	3.46	3.46
Map sharpening B-factor (Å^2)	-124.4	-108.9	-85.9	-140.5	-154.1	-142.1	-159.6	-148.7

[a] For clarification, "Acid_" is omitted from dataset names.
[b] Approximate time from the initiation of acid treatment to the state of being quenched by freezing.
[c] Three structural states are Native (full native virions), E1 (expanded 1 particles), and A- (A-particles).
[d] Micrographs from which particles were selected.
[e] Mean±SD: 3.9±1.6 (Acid_A_1), 3.3±1.3 (Acid_A_2), 3.1±0.7 (Acid_A_3), 3.1±0.8 (Acid_A_4).
[f] Estimated based on Fourier shell correlation between two half maps using a cutoff of 0.143 (69).

Table S5. Cryo-EM data statistics for dataset B_4_Neu.

	full_1	full_2	full_3	emp_1	emp_2	emp_3
Data collection and processing[a]						
(Probable) identity of the state	Full native	Expanded 1	A-particle	Emptied particle	Abortive product 1[f]	Abortive product 2[f]
No. of micrographs[b]	1767	1767	1767	1767	1767	1767
Defocus (μm)	0.9-5.9	0.9-6.0	0.9-5.9	0.9-6.0	0.9-5.9	0.9-5.9
Pixel size (Å/pixel)	1.62	1.62	1.62	1.62	1.62	1.62
Dose rate (e^-/pixel/s)	8	8	8	8	8	8
Frame rate (ms)	250	250	250	250	250	250
Total dose (e^-/ Å^2)	45	45	45	45	45	45
No. of particles obtained after 3D classification	124,865 (52.6%)	10,935 (4.6%)	20,755 (8.7%)	47,523 (20.0%)	16,981 (7.2%)	16,381 (6.9%)
No. of particles for reconstruction	10,000	10,935	20,000	20,000	13,000	13,000
Resolution[c] (Å)	3.24	3.31	3.24	3.32	3.24	3.24
Map sharpening B-factor (Å^2)	-155.6	-162.6	-161.7	-175.1	-157.1	-157.7
Model Statistics						
Correlation coefficient[d]	0.855	0.843	0.842	0.822	0.850	0.852
No. of atoms (protein)	6262	6001	5414	5124	5772	5638
Avg. B-factor (Å^2)	33.5	44.7	40.4	56.0	34.5	32.4
R.M.S.D. Bond lengths[e] (Å)	0.009	0.012	0.010	0.009	0.008	0.008
R.M.S.D. Bond angles[e] (°)	1.203	1.271	1.225	1.205	1.188	1.184
Ramachadran plot favored[e] (%)	94.7	94.5	93.2	93.1	95.6	94.1
Ramachadran plot allowed[e] (%)	5.3	5.5	6.6	6.7	4.4	5.8
Ramachadran plot outliers[e] (%)	0.0	0.0	0.2	0.2	0.0	0.1

[a] Cryo-EM data were collected using an FEI Titan Krios transmission electron microscope operated at 300 kV and equipped with a Gatan K2 Summit direct electron detector.
[b] Micrographs from which particles were selected.
[c] Estimated based on Fourier shell correlation between two half maps using a cutoff of 0.143 (69).
[d] Between cryo-EM map and a map calculated based on the atomic model specifying the cryo-EM map resolution.
[e] Based on the criteria of MolProbity (76).
[f] Abortive 1 probably represents native empty particles, while Abortive 2 contains rod-like inner densities.

Table S6. Root-mean-square deviations (Å) between pairs of structures (dataset B_4_Neu).[a]

	Full native	Expanded 1	A-particle	Emptied particle	Abortive product 2	Abortive product 1
Full native	-					
Expanded 1	4.4	-				
A-particle	6.0	3.3	-			
Emptied particle	4.9	1.1	1.1	-		
Abortive product 2	1.0	3.5	4.3	4.0	-	
Abortive product 1	1.1	3.5	4.3	4.0	0.3	-

[a] Calculated based on equivalent Cα atoms when icosahedral symmetry axes are aligned.

Table S7. Rigid body movements of capsid proteins when full native virions are converted into E1 particles.

Protein	Psi[a] (°)	Phi[a] (°)	Kappa[b] (°)	Translation (Å)	r.m.s.d.[c] (Å)
VP1	77.0	38.0	2.8	4.5	1.1
VP2	83.5	17.5	3.3	3.4	1.3
VP3	71.6	15.2	2.8	3.9	1.4
VP4	48.7	40.8	3.3	4.7	0.3

[a] These two polar angles define the direction of the rotational axis according to (81).
[b] Clockwise rotation as viewed out from inside the virus.
[c] Between equivalent Cα atoms.

Table S8. Buried surface areas (Å^2) at the intra-protomer protein-protein interacting interfaces.[a]

Structure	Interfaces					
	VP1-VP3	VP1-VP2	VP2-VP3	VP1-VP4	VP3-VP4	VP2-VP4
Full native	4347.7	1931.2	1701.8	840.3	768.6	293.6
Expanded 1	3849.0	1978.0	1684.6	836.3	746.1	307.3
A-particle	3048.0[b]	1624.6	1713.8	-	-	-
Emptied particle	2511.6	1636.9	1687.2	-	-	-
Full native-Expanded 1[c]	3959.9	1948.2	1701.8	840.3	747.0	293.6
Expanded 1-A-particle[c]	2681.7[b]	1656.4	1737.9	-	-	-
A-particle-Emptied[c]	2538.0	1632.6	1686.5	-	-	-

[a] The buried surface areas were calculate using the program PISA (79).
[b] The interactions between the externalized VP1 N-terminus and the VP3 GH loop contribute to an increase of the VP1-VP3 interaction area in A-particles with respect to E1-particles.
[c] A-B refers to a modified structure of A in which only atoms equivalent to B are retained.

Table S9. Comparison of buried surface areas at the interpentamer interfaces.

Genus	Species	Virus	PDB	Buried surface Area[a] (Å^2)	Acid labile?
Enterovirus	Enterovirus A	EV-A71	3ZFE	5982.1	No
		CV-A16	5C4W	5796.0	No
	Enterovirus B	CVB3	4GB3	5411.4	No
		CVA9	1D4M	5147.6	No
	Enterovirus C	PV1	1ASJ	5332.0	No
		PV3	1PVC	5125.3	No
	Enterovirus D	EV-D68 (Fermon)	4WM8	5330.3	Yes
		EV-D68 (MO, A_Native)	6CSG	5046.4	Yes
	Rhinovirus A	RV-A16	1AYM	4751.6	Yes
		RV-A2	1FPN	4605.5	Yes
	Rhinovirus B	RV-B3	1RHI	5123.1	Yes
		RV-B14	4RHV	5112.0	Yes
	Rhinovirus C	RV-C15	5K0U	4613.2	Yes
Aphthovirus	Foot-and-mouth disease virus (FMDV)	FMDV[c]	1BBT	4599.5	Yes
Cardiovirus	Encephalomyocarditis virus	Mengovirus[d]	2MEV	4774.8	Yes
Structural states of EV-D68 (Dataset B_4_Neu)		Full native	6CRR	5183.7	
		Expanded 1	6CS3	3555.0	
		A-particle	6CRS	2925.9	
		Emptied particle	6CRU	2482.5	

[a] Calculated using the program PISA (79).
[b] To be assigned by the Protein Data Bank.
[c] Acidification causes dissociation of the capsid into pentamers (82).
[d] The capsid is broken apart to form pentamers under low pH and in the presence of halide anions (52).

Table S10. Acid labile enteroviruses possess more histidines in capsid proteins than acid resistant enteroviruses.[a]

Species	Virus	PDB	Total No. of amino acids[b]	No. of His	Mean No. of His	Acid lability?
Enterovirus A	EV-A71	3ZFE	862	18	19	Resistant
	CV-A16	5C4W	862	21		
Enterovirus B	CVB3	4GB3	850	17		
	CVA9	1D4M	866	22		
Enterovirus C	PV1	1ASJ	880	19		
	PV3	1PVC	878	17		
Enterovirus D	EV-D70[c]	-	866	17		
	EV-D68[d]	4WM8	860	26	25	Labile
Rhinovirus A	RV-A16	1AYM	852	26		
	RV-A2	1FPN	855	25		
Rhinovirus B	RV-B3	1RHI	854	23		
	RV-B14	4RHV	855	24		
Rhinovirus C	RV-C15	5K0U	841	27		

[a] $P<0.0001$ by unpaired Student's *t* –test. The extra histidine residues in acid sensitive EVs are primarily found in VP1 and VP2.

[b] Total number of amino acids in capsid proteins including VP1, VP2, VP3, and VP4.

[c] Like EV-D70, EV-D94 is also acid resistant and contains 16 histidines.

[d] This refers to the Fermon strain. Strains MO and KY both contain 26 histidines.

Table S11. Differences of amino acid sequences in capsid proteins among members of the EV-D species.

Residue No.[a]	EV-D94[b]	EV-D70[b]	EV-D68[c]	Occurrence of His[d] (%)	Location on virus	2nd most common residue[d]
1162	E	E	H	100.0	Close to quasi-three-fold axis	
1228	Y	Y	H	100.0	Close to quasi-three-fold axis	
1292	N	N	H	99.6	Close to five-fold axis	
2045	N	N	H	99.6	Interior	
2098	Y	Y	H	93.5	Near two-fold axis	Y (6.5%)
2135	Y	K	H[e]	81.0	At junction of VPs in a protomer	Y (19.0%)
2244	N	N	H	100.0	Near two-fold axis	
3238	Q	I	H	99.8	At junction of VPs in a protomer	
3240	E	P	H	84.7	At junction of VPs in a protomer	D (15.1%)
4023	N	S	H	100.0	Interior	

[a] Numbering based on the amino acid sequence of EV-D68 strain MO.
[b] GenBank accession numbers are ABL61316.1 and ABA43708.1 for EV-D94 and EV-D70. They share about 76% amino acid sequence identity with EV-D68 strain MO in the capsid region.
[c] Strains MO and KY possess the same set of ten histidines shown here. Strain Fermon has one exception which is a Tyr at position 2098.
[d] Among 469 EV-D68 strains for which a complete or nearly complete genome sequence is available in GenBank.
[e] In close proximity to the conserved His2157.

Supplementary References

81. Rossmann MG, Blow DM (1962) The detection of sub-units within the crystallographic asymmetric unit. *Acta Crystallogr* 15:24-31.
82. Cavanagh D, Rowlands D, Brown F (1978) Early events in the interaction between foot-and-mouth disease virus and primary pig kidney cells. *J Gen Virol* 41(2):255-264.